DTC Visitor Program Final Report

Evaluating CCPP Physics Across Scales for Severe Convective Events

William A. Gallus, Jr., Iowa State University

Introduction

With the recent development of the Unified Forecast System (UFS), the dynamic cores of many NCEP operational models are being replaced with the Finite-Volume Cubed -Sphere (FV3) model. Already, the FV3 has been implemented in the GFS model, which is run with a relatively coarse horizontal grid, requiring the use of convective parameterization. Eventually, as the FV3 core replaces the WRF core in the HRRR, the model will be running with a range of horizontal grid spacings, including down to convection-allowing grid spacings on the order of 3 km. The ideal situation with such a model is to have a scale-aware physics suite that can be used for all of these horizontal grid spacings.

Some testing has already been performed by the DTC group to investigate how scale-aware two physics suites are in the FV3 model for a range of meteorological situations, using the limited area version of the model (FV3-LAM) which allows for fine grid spacings to be used. The goal of the present project was to test the FV3-LAM with three horizontal grid spacings, 3 km, 13 km, and 25 km, to simulate three convective events, one being a system well-simulated in earlier work using the WRF model, another being a poorly simulated case with the WRF model, and a third where the skill of the WRF simulations depended on the microphysics scheme used. The two physics suites tested were the GFSv16beta and the RRFSv1beta. Events were chosen to include bow echo and trailing stratiform squall line morphologies, as the prior work of the PI (e.g., Snively and Gallus 2014; Thielen and Gallus 2019) showed that these morphologies were most poorly predicted by convection-allowing models.

Methodology

To ensure that output was available for initial conditions and lateral boundary conditions in a form acceptable for use in the FV3-LAM, a few of the cases originally planned to be the focus of the study had to be replaced with more recent events. A squall line with some evidence of bowing that occurred in western Texas on May 20, 2019, was chosen as the well-predicted case, based on a quick analysis of prior HRRR runs. A bow echo case that occurred on June 2, 2015 was chosen as a mixed case, where the skill of earlier WRF simulations performed by the PI's research group was very dependent upon the microphysics scheme used. Finally, the very destructive Midwestern derecho of August 10, 2020, was chosen as a poorly predicted case since the majority of convection-allowing models run for that event in real time performed poorly. The 2015 and 2019 cases were initialized at 1200 UTC using NAM output. For the 2020 derecho case, initialization occurred at 0000 UTC, and HRRRv4 (experimental HRRR at the time) output was used for IC/LBCs since the 0000 UTC runs of the HRRR and HRRRx were the only 0000 UTC models run in real time that did not produce spurious convection in the first 12 hours of the simulation (overnight period) and showed some evidence of an organized convective system crossing Iowa around the time the derecho was observed. All runs were integrated for 24 hours, as the primary convective system of interest occurred mostly 12-24 hours after model initialization.

The FV3-LAM runs used a CONUS domain. For the 2015 and 2019 cases, the Grell-Freitas (GF) convection scheme was only used in the RRFS physics suites for the 25 and 13 km horizontal grid spacing runs. However, for the August 2020 derecho case, a test was run where GF was also used at 3 km. In addition, for that case, runs were also performed with GF neglected at both 13 and 25 km grid spacing. The GFS physics suite used the SAS (Simplified Arakawa-Schubert) scheme in all runs.

A python script was used to visualize simulated reflectivity for all cases, and ncl scripts were used to plot 2m temperature, 10 m wind, 850 mb vertical motion, heights and winds, CAPE, and total accumulated and convective precipitation for some events to better understand the simulated evolution. In addition, MET (Model Evaluation Tools) and METviewer were used to perform more quantitative verification, usually over a small domain centered on the event of interest. Traditional point-to-point measures such as mean error and frequency distributions were examined for reflectivity, temperature, dew point, relative humidity, and wind speed

Results

Although the goal of the project was to understand general trends in the behavior of the physics suites for the three convective cases at different horizontal grid spacings to evaluate how scale-aware they were, it was discovered that the FV3-LAM runs exhibited very unusual behavior in their simulations of the 2020 derecho event. Thus, much deeper evaluation was performed for that event and a paper on it has been submitted to Weather and Forecasting, where it has been conditionally accepted (Gallus and Harrold, 2023). In the discussion to follow, the general results will be presented in the first subsection, with additional discussion of the derecho results following in a second subsection.

a) General evaluation of scale-awareness

Frequency bias (FBIAS) for reflectivity for small domains centered on the convective systems of interest (Fig. 1) shows that the 3 km GFS physics suite runs have the highest bias, usually followed by the 3 km RRFS run (without the GF cumulus scheme). For the derecho case, the 3 km RRFS with the GF scheme has a smaller bias than the 3 km run without GF. The 25 km RRFS always has the lowest FBIAS, and the 13 km RRFS is often second lowest (both of these runs used the GF cumulus scheme). When GF is turned off in these coarser grid spacing runs for the 2020 derecho case, FBIAS increases. In all 3 cases, the main convective event of interest is in the last 12 hours of the forecast period. During this active period, the high biases in the 3 km runs are greatly reduced. In the 2020 and 2019 cases, it is only the 3 km runs prior to the convective event of interest that have FBIAS greater than 1.0. During the main convective events, all runs have smaller reflectivity coverage than observed. In the 2015 case, FBIAS values exceed 1.0 for longer periods and in almost all of the runs, but again primarily before the main convective event. Because of the complexity of the 2020 event (discussed in the next subsection), the runs that had the highest FBIAS prior to the main convective event had the lowest FBIAS values with great underestimates of the coverage of reflectivity later in the simulation when the derecho event was most active.

Mean errors for temperature (Fig. 2) depict great variability among the cases. The 3 km runs tend to be coldest, although the 3km RRFS run for the 2020 event with the GF scheme on was less cold. The GFS runs at 13 and 25 km are often warmest. The 2015 case has generally positive (warm) errors, while the other two cases are usually colder than observed, except for the 2020 derecho event in the afternoon, when the errors are usually positive.

a)

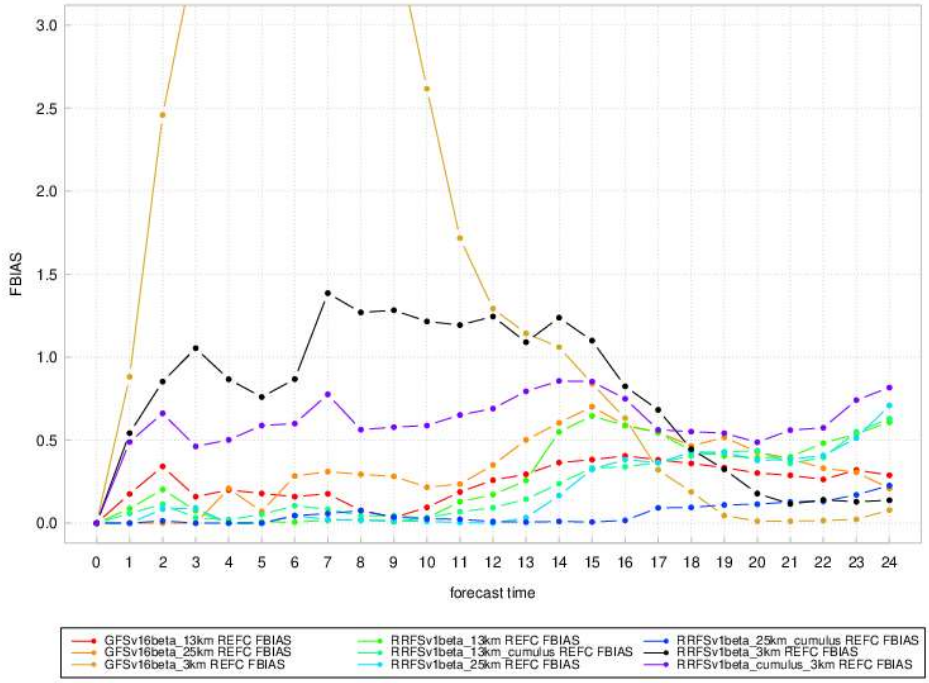
REFC FBIAS 2020
FBIAS
forecast time
GFSv16beta_13km REFC FBIAS
GFSv16beta_25km REFC FBIAS
GFSv16beta_3km REFC FBIAS
RRFSv1beta_13km REFC FBIAS
RRFSv1beta_13km_cumulus REFC FBIAS
RRFSv1beta_25km REFC FBIAS
RRFSv1beta_25km_cumulus REFC FBIAS
RRFSv1beta_3km REFC FBIAS
RRFSv1beta_cumulus_3km REFC FBIAS

b)

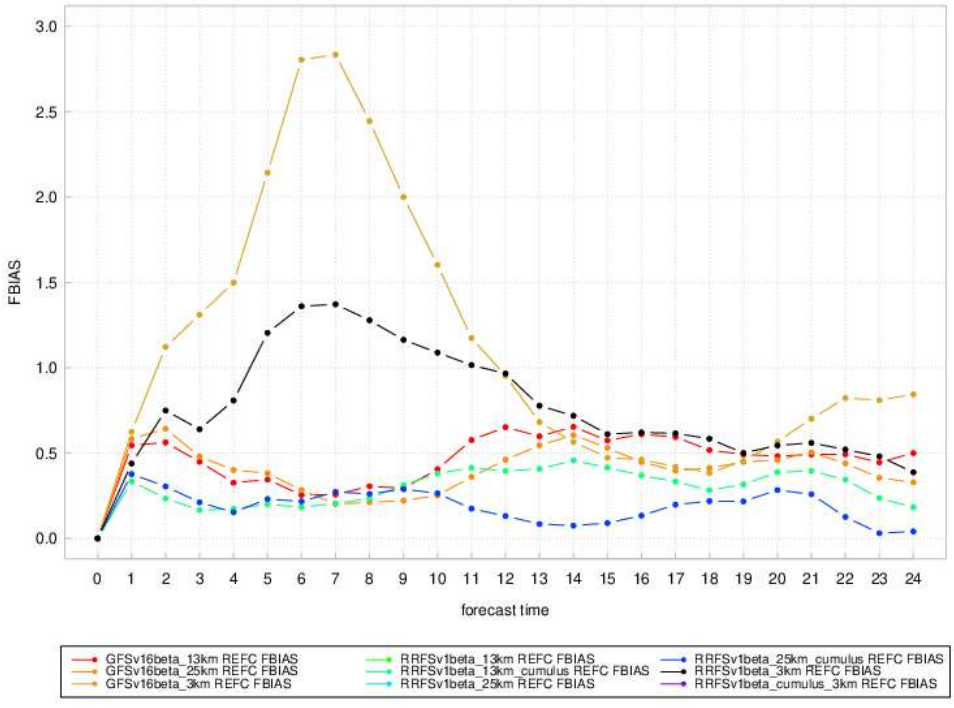
REFC FBIAS May 2019
FBIAS
forecast time
GFSv16beta_13km REFC FBIAS
GFSv16beta_25km REFC FBIAS
GFSv16beta_3km REFC FBIAS
RRFSv1beta_13km REFC FBIAS
RRFSv1beta_13km_cumulus REFC FBIAS
RRFSv1beta_25km REFC FBIAS
RRFSv1beta_25km_cumulus REFC FBIAS
RRFSv1beta_3km REFC FBIAS
RRFSv1beta_cumulus_3km REFC FBIAS

c)

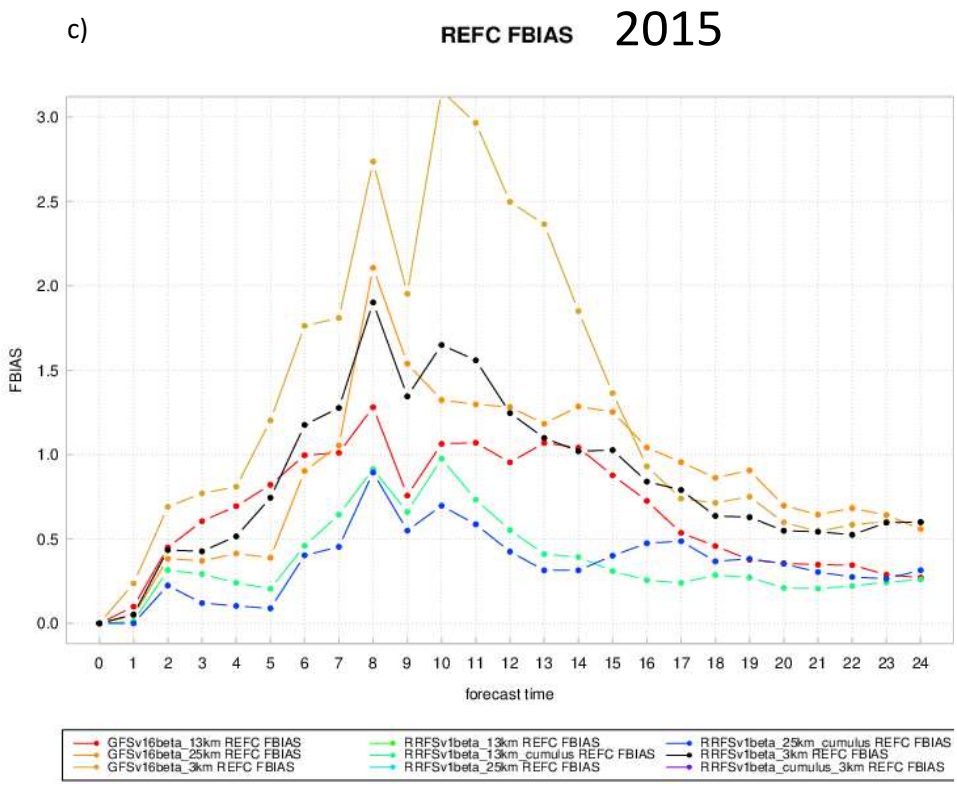

Figure 1: Frequency bias for reflectivity for the a) August 10, 2020 derecho case, b) May 20, 2019 Texas squall line, and c) June 2, 2015 Northern Plains bow echo for each hour of the simulations (defined by color bar below each figure). Red is for the 25 km GFS run, orange is the 13 km GFS run, tan the 3 km GFS run, dark blue is RRFS with the GF scheme at 25 km, light blue is 25 km RRFS without the GF scheme, green is the 13 km RRFS run with the GF scheme, light green the 13 km RRFS without GF, purple is the 3 km RRFS with the GF scheme, and black the 3 km RRFS without GF.

a)

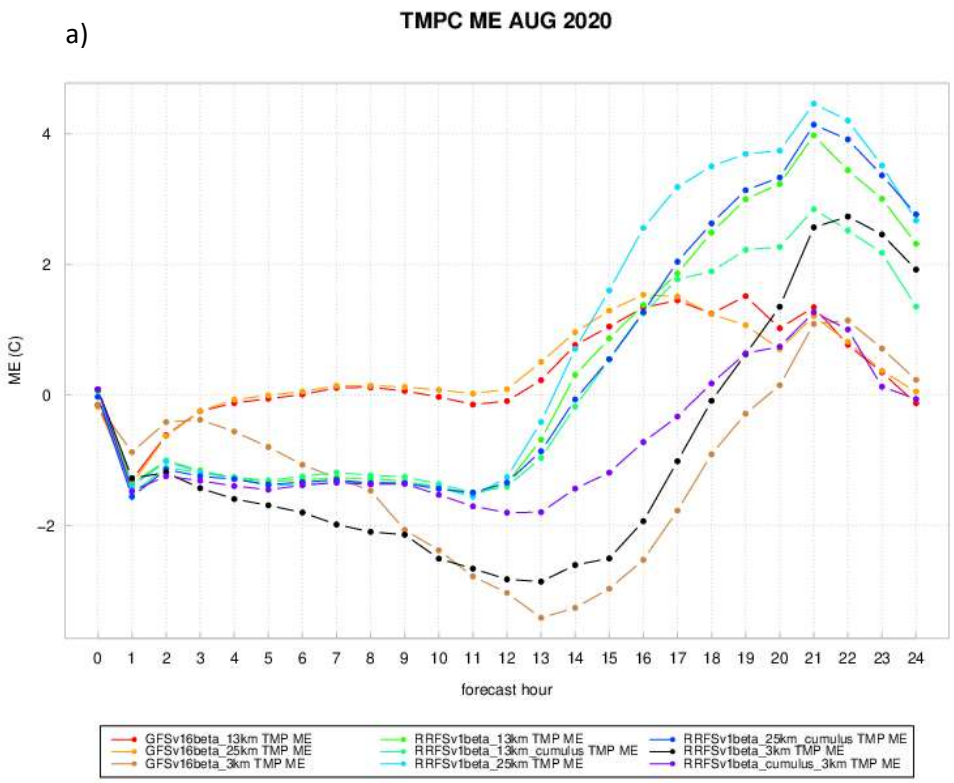
TMPC ME AUG 2020
ME (C)
forecast hour
GFSv16beta_13km TMP ME
GFSv16beta_25km TMP ME
GFSv16beta_3km TMP ME
RRFSv1beta_13km TMP ME
RRFSv1beta_13km_cumulus TMP ME
RRFSv1beta_25km TMP ME
RRFSv1beta_25km_cumulus TMP ME
RRFSv1beta_3km TMP ME
RRFSv1beta_cumulus_3km TMP ME

b)

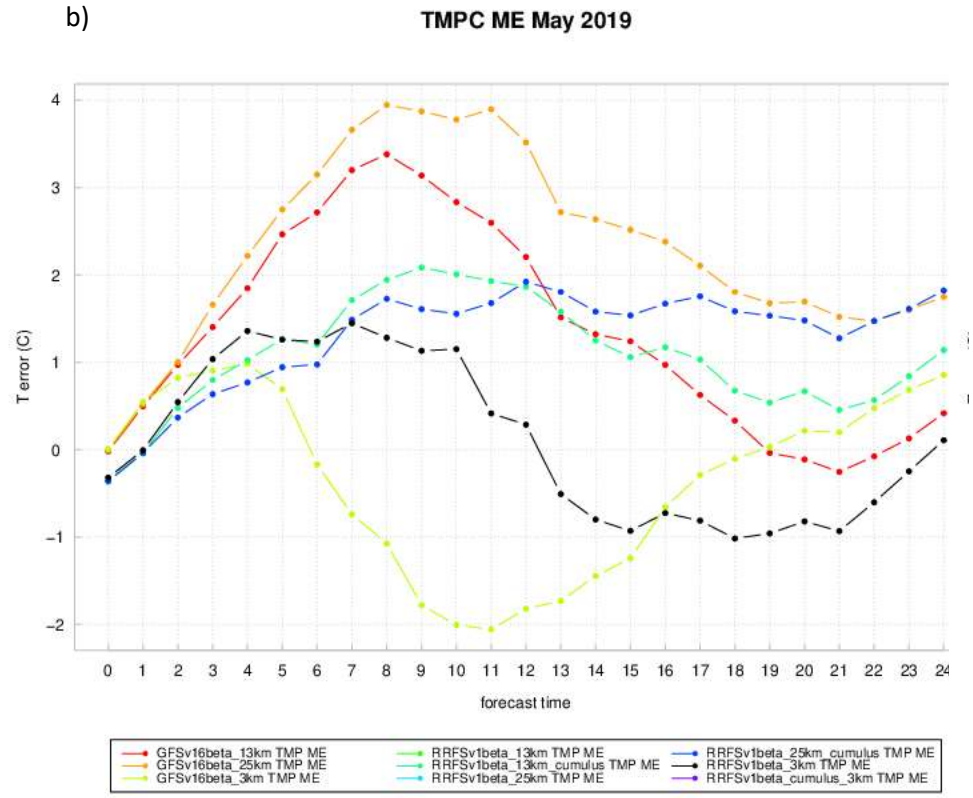
TMPC ME May 2019
T error (C)
forecast time
GFSv16beta_13km TMP ME
GFSv16beta_25km TMP ME
GFSv16beta_3km TMP ME
RRFSv1beta_13km TMP ME
RRFSv1beta_13km_cumulus TMP ME
RRFSv1beta_25km TMP ME
RRFSv1beta_25km_cumulus TMP ME
RRFSv1beta_3km TMP ME
RRFSv1beta_cumulus_3km TMP ME

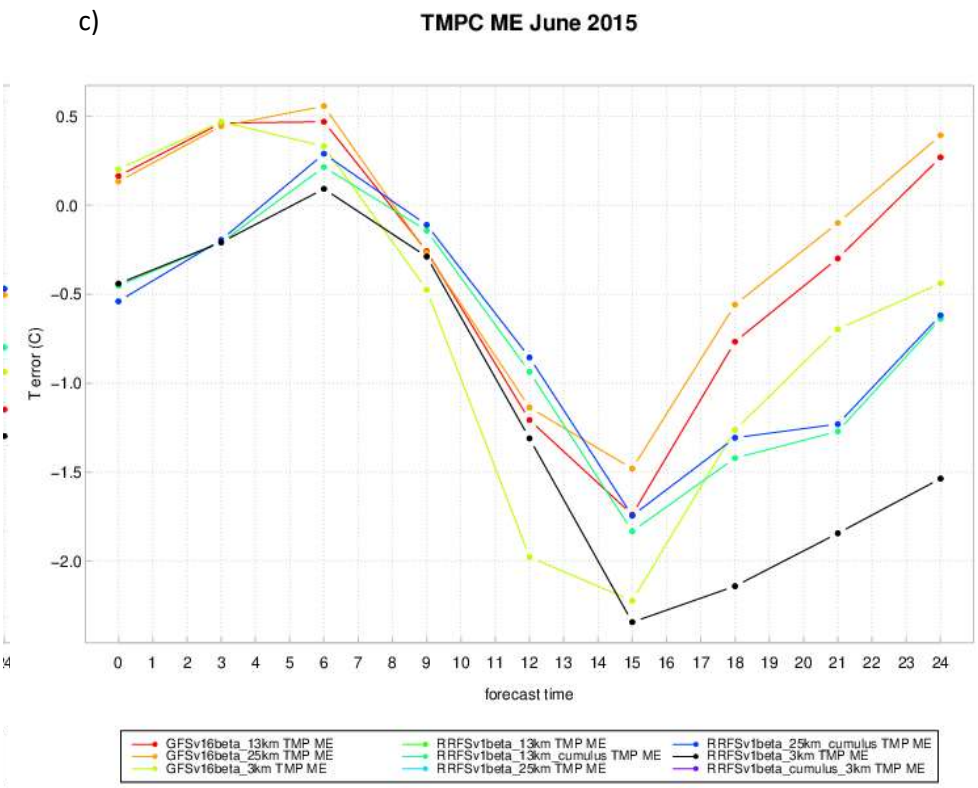

Figure 2: As in Fig. 1 but for mean error (C) for 2m temperature.

More variability exists in the 2 m dew point errors among runs and cases (Fig. 3), although most of the model runs tend to have a positive bias. The 3 km runs are drier much of the time, but the 3 km GFS run is among the moistest for the June 2015 case early on. The 13 and 25 km runs with GFS are often among the moistest but not always. The 2020 derecho case exhibits an especially large range in dew point errors, with some of the 25 km runs have positive errors as large as 2 C, with some 3 km runs having negative errors of 3-4 C.

Unlike the other weather parameters evaluated, 10 m wind errors do not differ noticeably among the different model runs (Fig. 4). The errors are relatively large, on the order of several knots, but vary greatly over time. The errors are always negative, and are as large as 6-8 knots for the 2019 and 2015 cases. The greatest underprediction of wind speed happens at 21 UTC in the afternoon for all 3 cases. The wind errors are 1-3 knots less during the night than they are during the afternoon.

The ratio of total precipitation to convective component varies among cases. For the 2015 northern Plains event, the 25 km and 13 km runs with RRFS and GFS physics suites evidence

a)

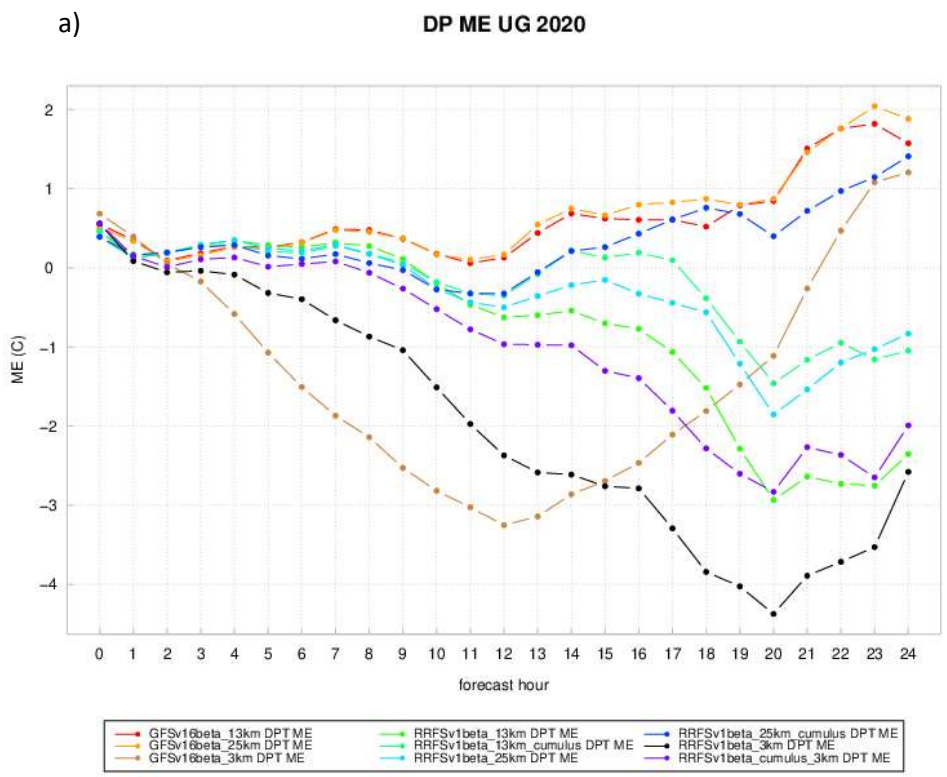
DP ME UG 2020
ME (C)
forecast hour
GFSv16beta_13km DPT ME
GFSv16beta_25km DPT ME
GFSv16beta_3km DPT ME
RRFSv1beta_13km DPT ME
RRFSv1beta_13km_cumulus DPT ME
RRFSv1beta_25km DPT ME
RRFSv1beta_25km_cumulus DPT ME
RRFSv1beta_3km DPT ME
RRFSv1beta_cumulus_3km DPT ME

b)

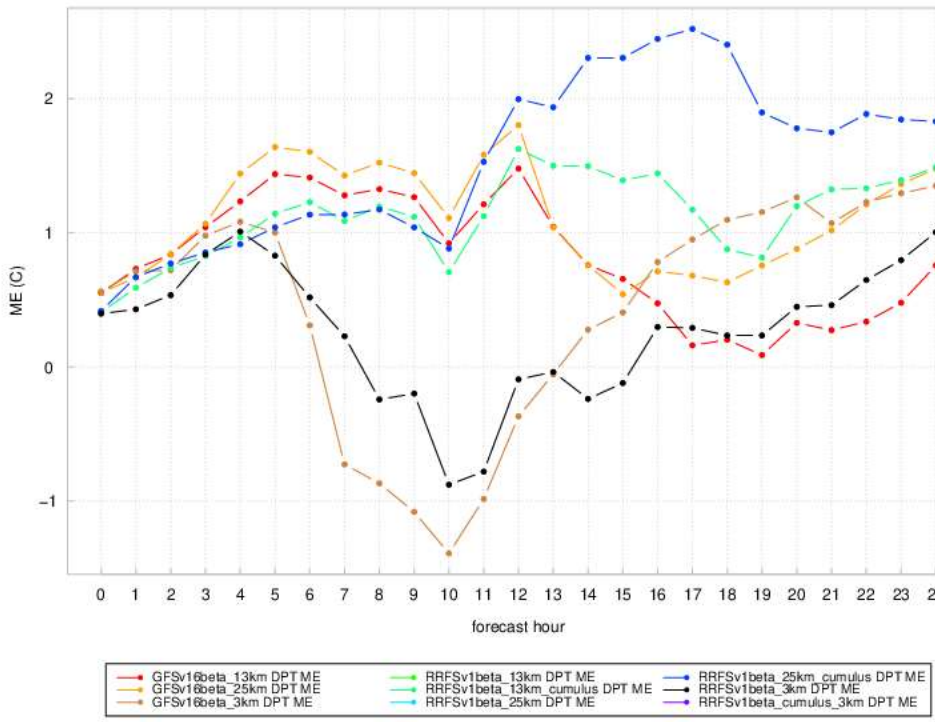
DP ME May 2019
ME (C)
forecast hour
GFSv16beta_13km DPT ME
GFSv16beta_25km DPT ME
GFSv16beta_3km DPT ME
RRFSv1beta_13km DPT ME
RRFSv1beta_13km_cumulus DPT ME
RRFSv1beta_25km DPT ME
RRFSv1beta_25km_cumulus DPT ME
RRFSv1beta_3km DPT ME
RRFSv1beta_cumulus_3km DPT ME

c)

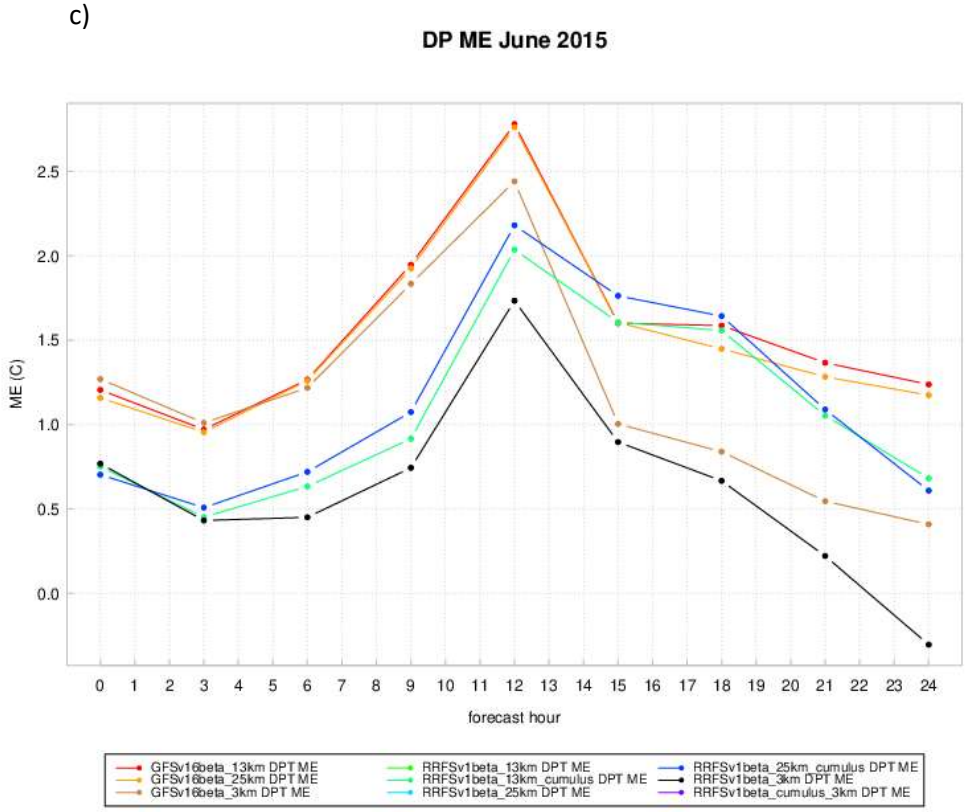

Figure 3: As in Fig 2 but for 2m dew point.

a)

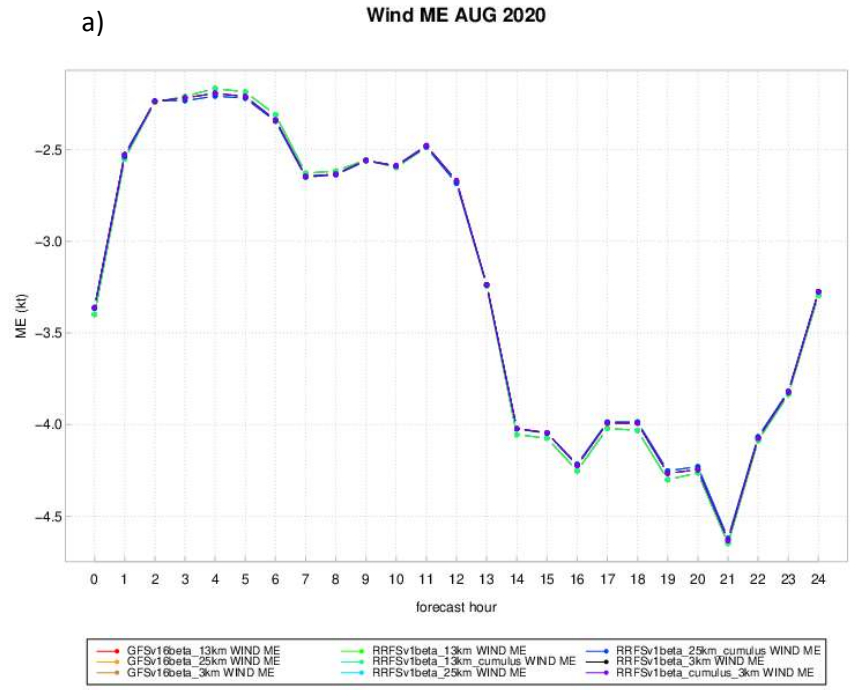

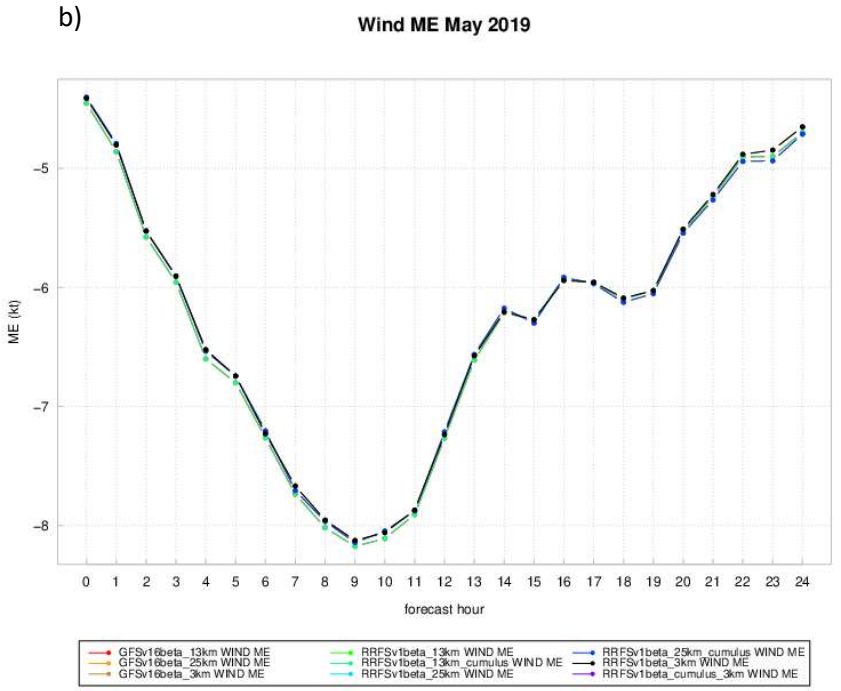

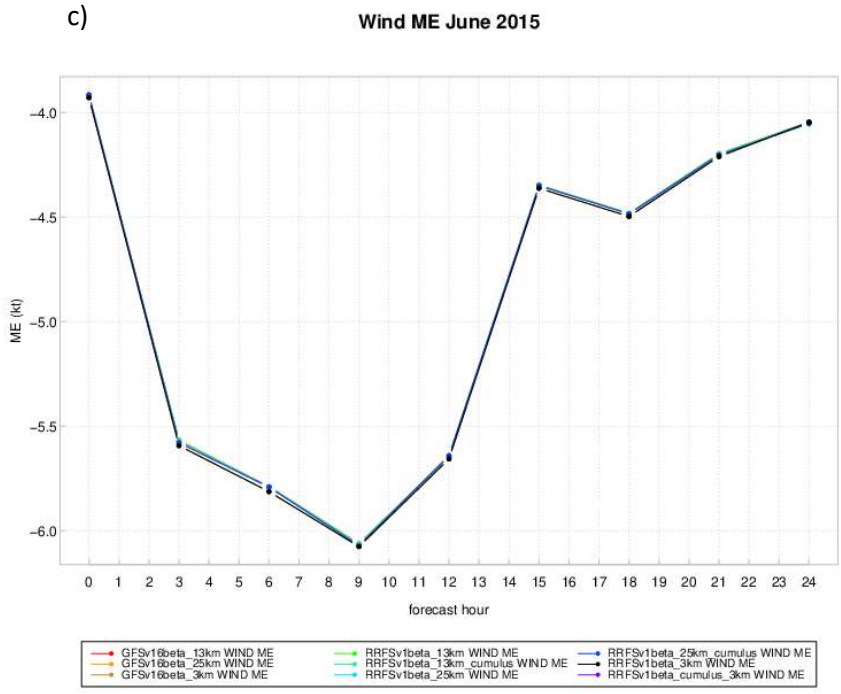

Figure 4: As in Fig. 2 but for mean error (kts) for 10 m winds.

much greater precipitation in the GFS runs, both from the SAS cumulus scheme and the explicit production (Fig. 5). At 25 km grid spacing, in the RRFS runs, only around 1 mm of precipitation comes from the GF scheme, with total precipitation only reaching 10-20 mm. The SAS scheme

in the GFS runs, however, produces up to 30 mm or so of rainfall, with the total precipitation reaching 60 mm or more. For the 13 km runs, again very little precipitation comes from the GF scheme, but a small area of much heavier explicit precipitation compared to the 25 km run does form in central SD, with peak values reaching 50 mm or so. Again, the GFS runs have much more convective and total precipitation. The peak amounts from the convective scheme are similar to those in the 25 km run, reaching around 30 mm, while the total precipitation now has maxima as large as 100 mm. When grid spacing was refined to 3 km, less change occurred in the total precipitation (Fig. 6), but the convective component from the SAS became negligible. Simulated reflectivity for this event (Fig. 7) suggests that the physics suites were not very scale aware. Although radar indicates that the convection in western NE and the Dakotas organized into a bow echo which made it to western Iowa by 09 UTC, both the 25 and 13 km runs failed to show any bow echo or convective development into eastern NE. However, the 3 km results with both physics suites were much different, showing some hint of a bowing system making it farther southeast, although still not particularly close to where convection was observed. The GFS runs which were overly broad at 25 and 13 km, depicted the best bow echo at 3 km.

Precipitation trends were similar for the 2019 case in Texas (not shown) to the 2015 event, except that one small region in the 13 km RRFS run did develop more intense explicit precipitation than in the GFS run. The GFS suite runs resulted in much larger coverage of light rainfall than the RRFS runs. Less differences occurred in the simulated reflectivity among the different runs than

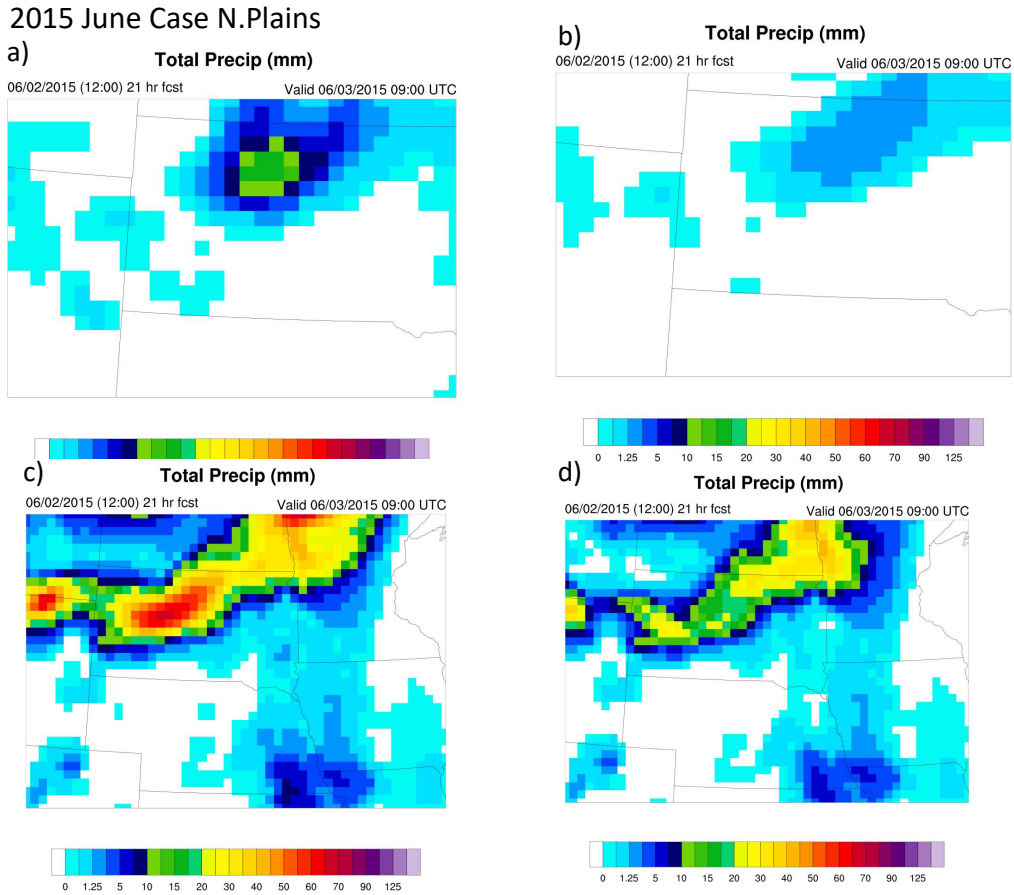

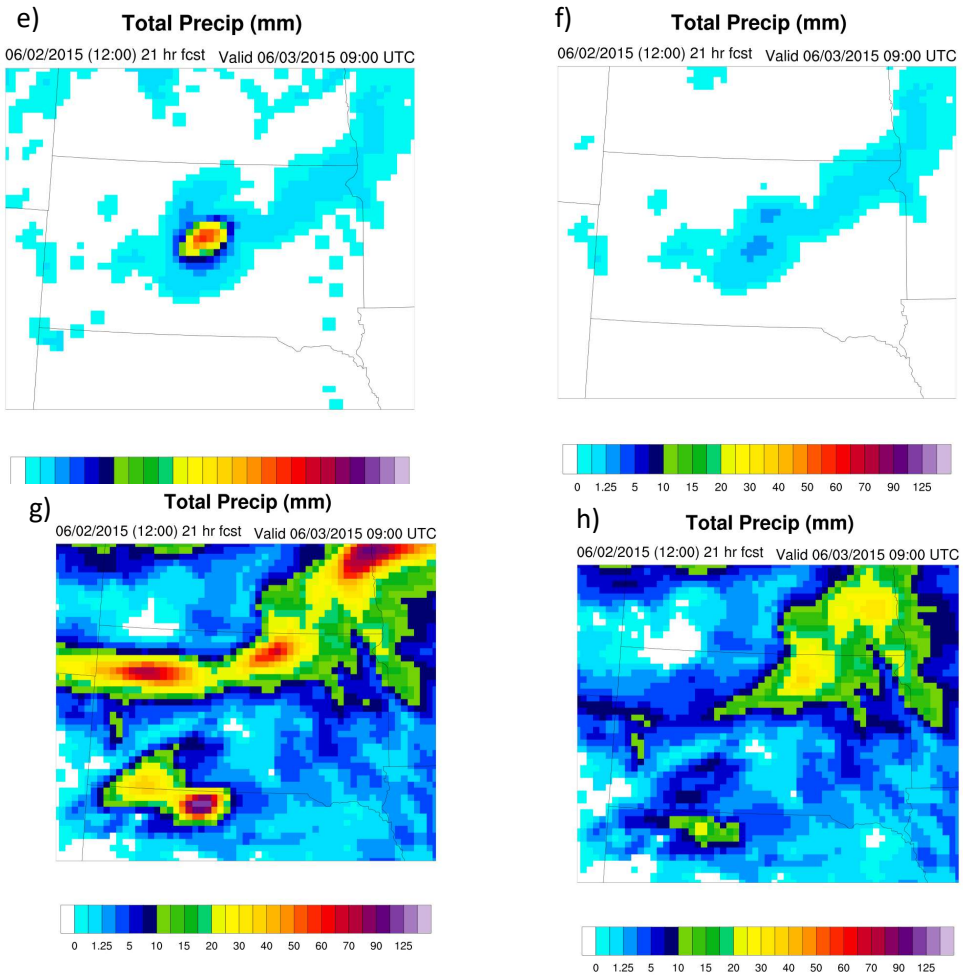

Figure 5: Total simulated rainfall (left, mm, see color bar) and convective component (right) for FV3-LAM runs initialized at 1200 UTC 2 June 2015 for 25 km runs using the RRFS physics suite (a, b) and the GFS suite (c, d), and 13 km runs using the RRFS physics suite (e, f) and GFS suite (g, h).

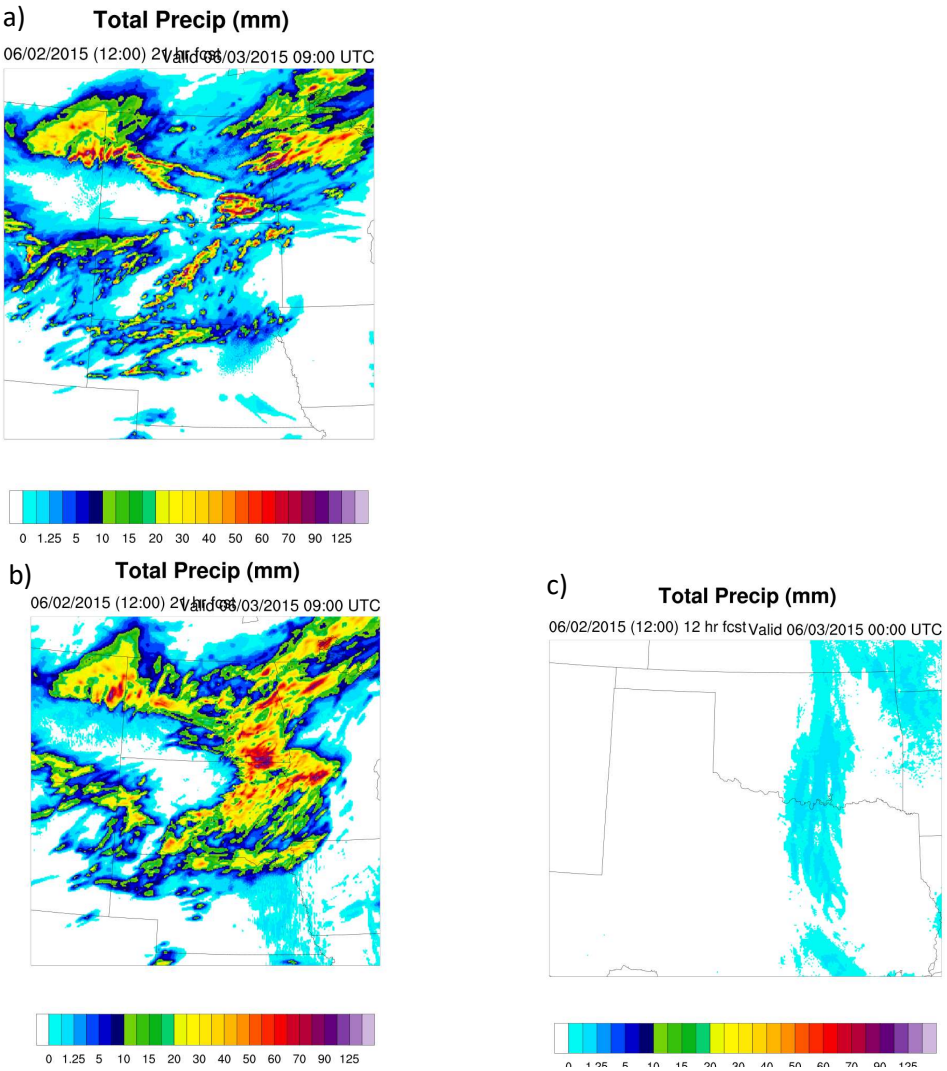

Figure 6:Total simulated rainfall (left, mm, see color scale) and the convective component (lower right) for 3km runs using the a) RRFS physics suite and (b, c) GFS suite for FV3-LAM runs initialized at 1200 UTC 2 June 2015. Note, no convective scheme was used in the RRFS physics suite run.

in the 2015 case (Fig. 8), with the locations of reflectivity being in generally the same regions, but the peak values were weaker in much of the line extending south across west Texas in the 13 and 25 km runs, as would be expected with coarse resolution of a narrow squall line. In addition, for this case, the RRFS suite resulted in a narrower line whereas the GFS suite seemed unable to have such fine details until the 3 km simulation.

Results for the 2020 derecho case are presented in Fig. 9. When the GF scheme was used in the RRFS suite, almost all of the precipitation in the 25 km run was produced by the GF scheme, and rainfall amounts were relatively light, under 15 mm (Figs. 9b, c). When the GF scheme was turned off in the 25 km run, peak amounts increased dramatically to around 100 mm (Fig. 9a). When the GFS suite was used (not shown), the convective component was much greater, up to 30 mm, with also a much larger explicit component, resulting in total rainfall approaching 100 mm, an

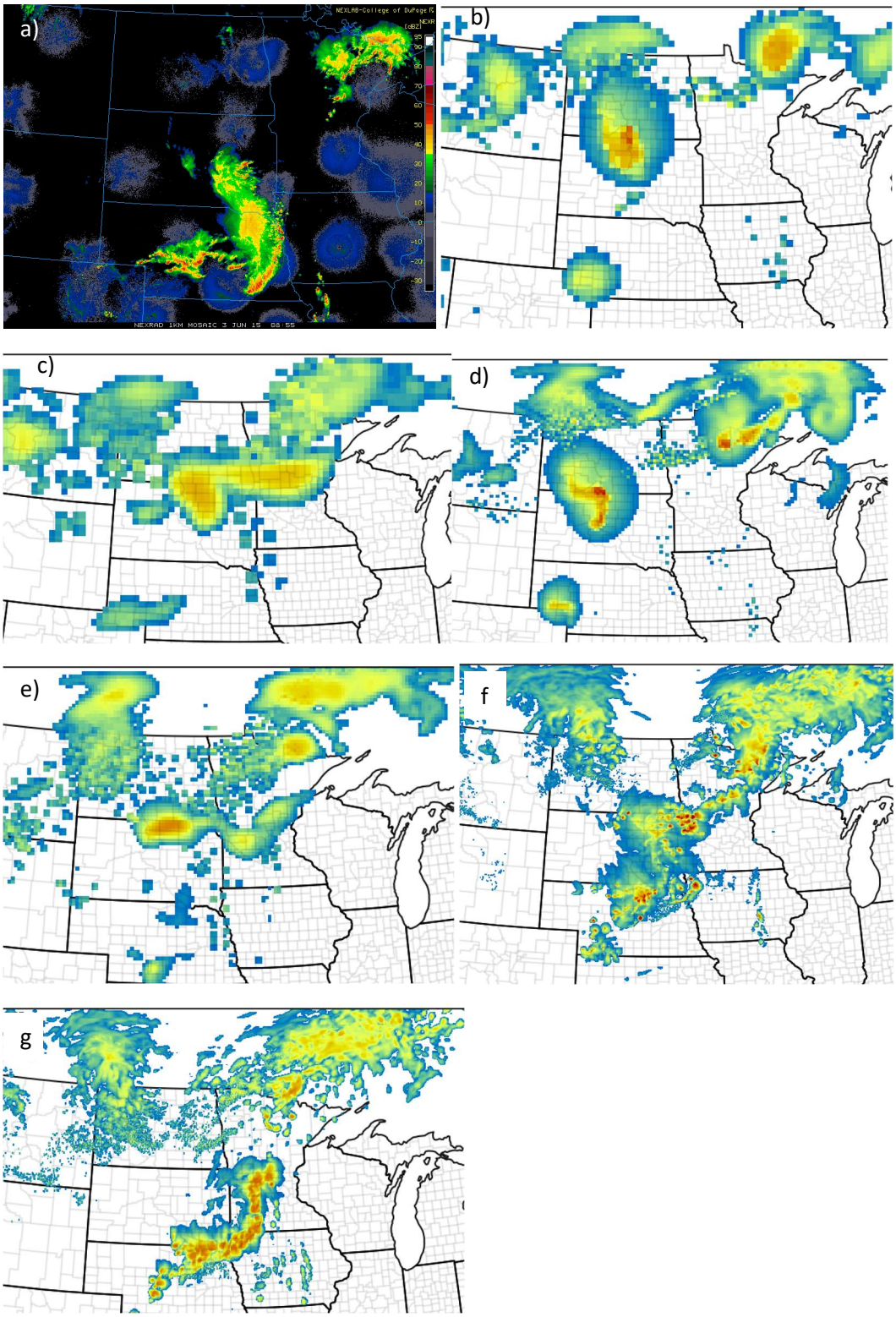

Figure 7: Observed radar (a) at 0900 UTC 3 June 2015, and simulated radar at the same time for b) 25 km RRFS, c) 25 km GFS, d) 13 km RRFS, e) 13 km GFS, f) 3 km RRFS, and g) 3 km GFS runs initialized at 1200 UTC 2 June 2015.

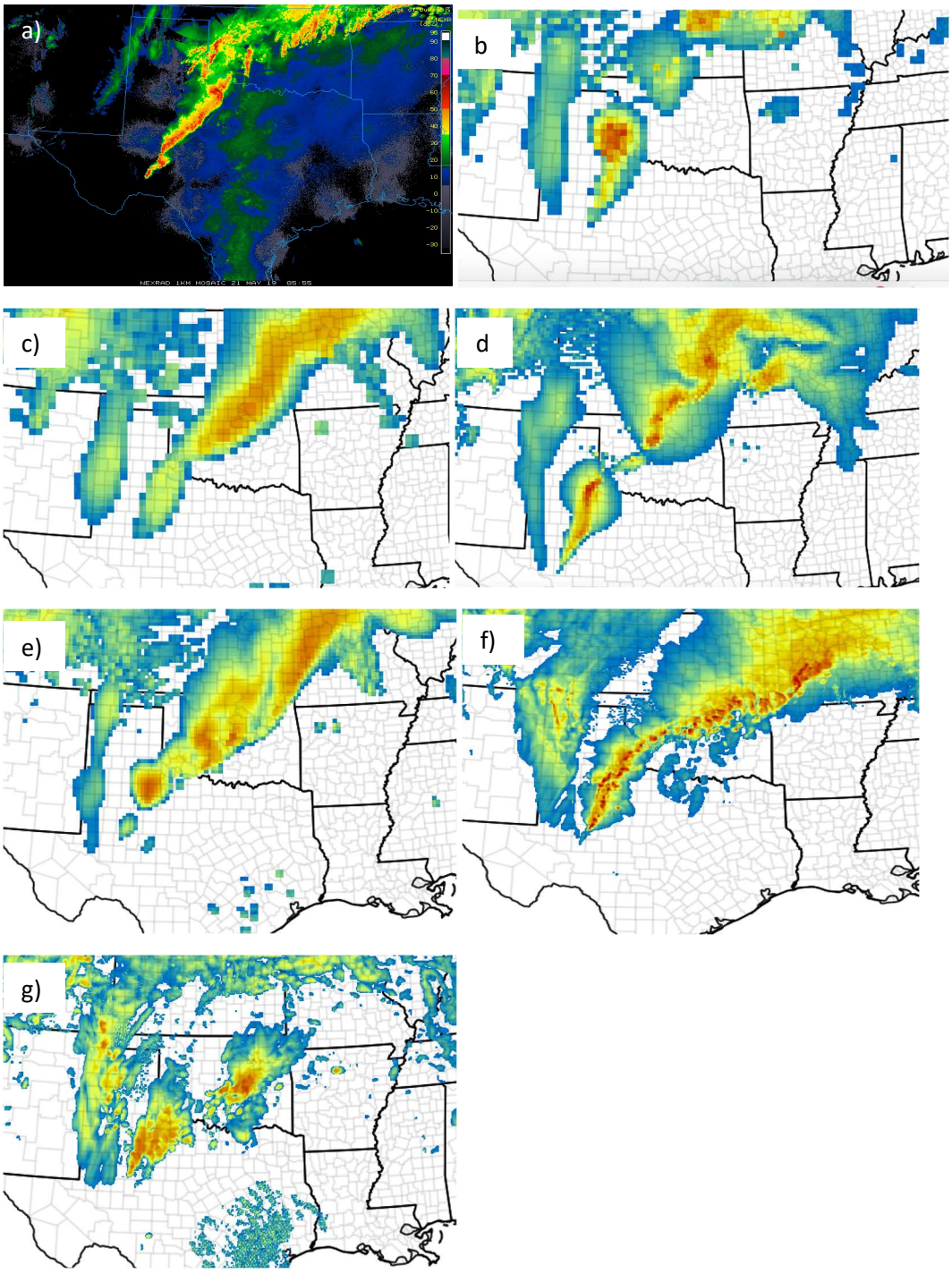

Figure 8: As in Fig. 7 but for 06 UTC 21 May 2019, for the case initialized at 12 UTC 20 May 2019.

amount similar to the RRFS run without the GF cumulus scheme. Both convective schemes resulted in larger areas of light rain than in the RRFS run that did not use the GF scheme.

When grid spacing was refined to 13 km, the convective component from the GF scheme did not change much from 25 km (Fig. 9f compared to Fig. 9c) but the total precipitation greatly increased

due to a much larger explicit component (Fig 9e). When the GF scheme was turned off, the areal coverage of light rainfall was reduced noticeably, and the peak amounts decreased slightly. It is also important to note that the location of the maxima also shifted several tens of kilometers. When the GFS suite was used (not shown), results did not change much from those shown on the 25 km grid. The convective component was reduced slightly, roughly 5 mm, while the total amount increased a similar small amount.

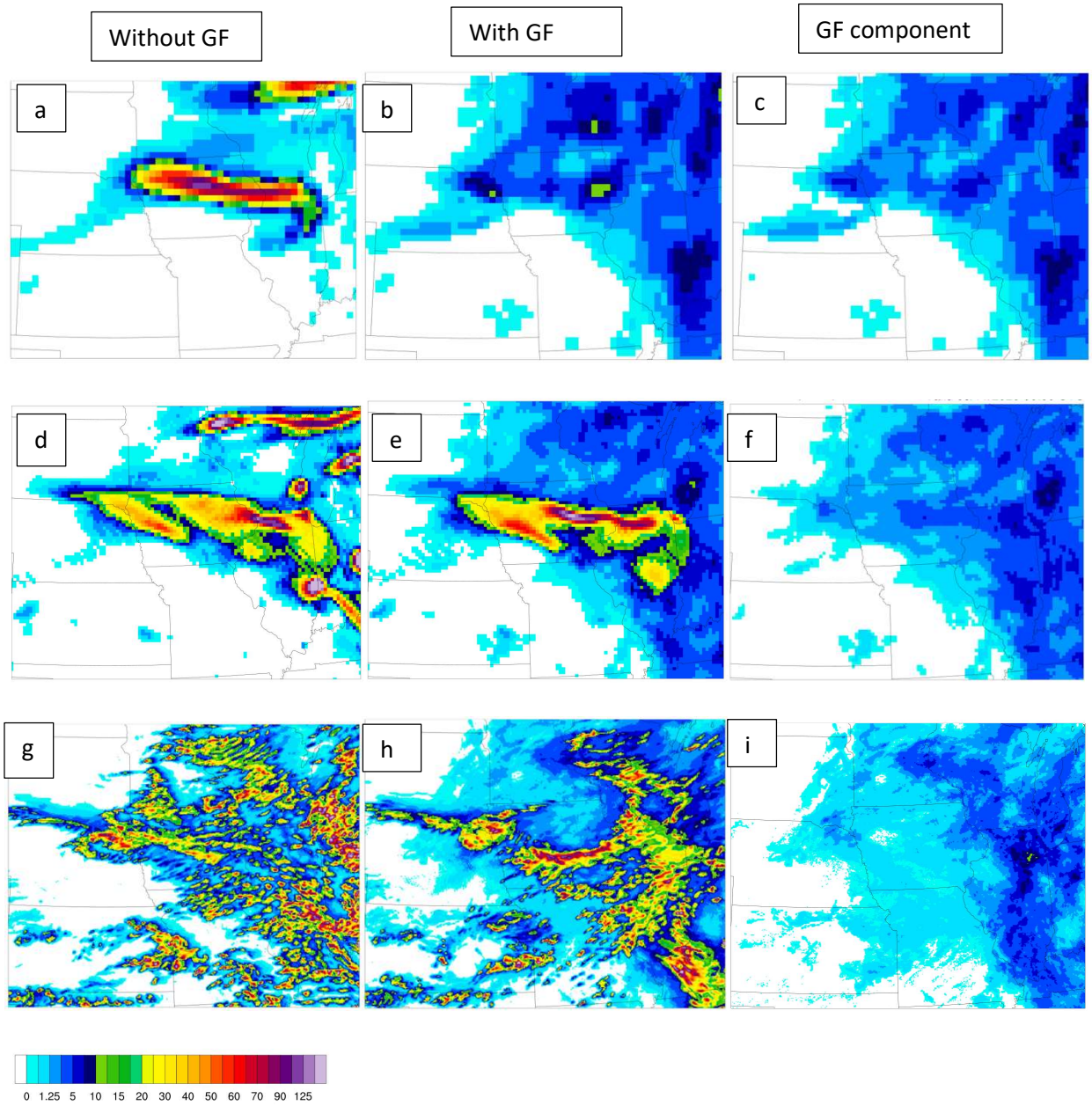

Figure 9: Total simulated rainfall (mm, see color bar) during the 0000 UTC 10 August – 0000 UTC 11 August period for the 25-km RRFS run a) without GF, b) with GF, and c) the convective component from GF, the 13-km RFFS run d) without GF, e) with GF, and f) the convective

component from GF, and the 3-km RRFS run g) without GF, h) with GF, and i) the convective component from GF.

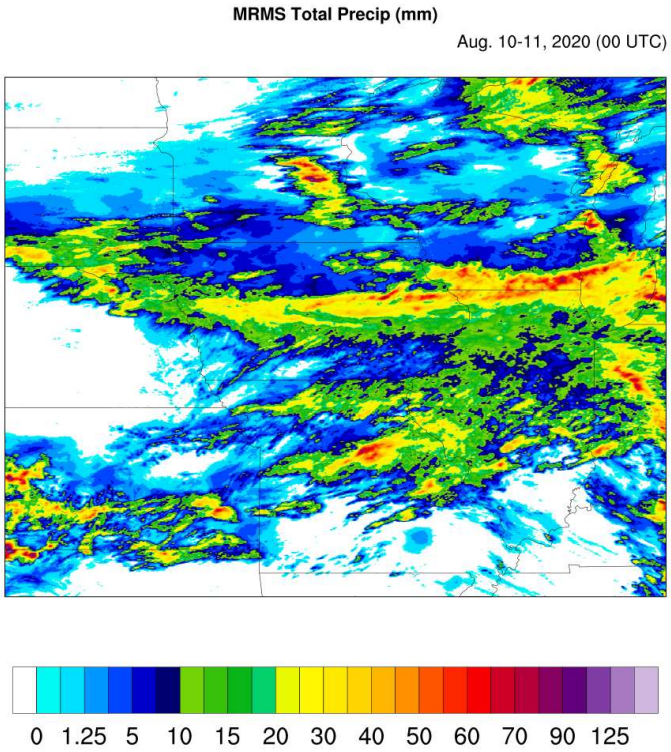

Figure 10: Observed precipitation (mm, from MRMS) from 0000 UTC 10 August to 0000 UTC 11 August 2020.

As will be discussed in more detail in the next subsection, very drastic changes happened in the precipitation in the 3 km runs when the GF scheme was turned on (Figs 9g-i) due to a completely different evolution of the convection. The component from the GF scheme was very small, not differing much from that of the 25 and 13 km simulations (Fig. 9i compared to Figs. 9c, f). The peak total amounts were slightly smaller than in the 13 km runs (Fig. 9h compared to Fig. 9e), and confined to smaller areas. When GF was not used, the 3 km results showed much less organization (Fig. 9g), with the heavier rain amounts displaced east into Illinois. The rainfall in Iowa generally occurred during the overnight hours and not when the derecho event actually occurred. The observed precipitation was generally less than the models indicated, with peak amounts of 50-75 mm (Fig. 10) but it was confined to a relatively narrow zone, and qualitatively matched best the 25-km run that did not use GF, both 13-km runs, and the 3-km run that did use GF. These were the runs that created a more intense system like that observed.

b) Detailed discussion of the FV3-LAM simulations of the August 2020 Midwestern derecho

As implied by some of the images in the previous subsection, FV3-LAM simulations of the August 2020 derecho exhibited some unusual behavior. Simulated reflectivity at 1800 UTC (around the time the observed derecho was producing its strongest winds near Cedar Rapids, IA), showed

large variations in the RRFS runs, depending on whether the GF scheme was being used (Fig. 11). For instance, in the 25 km runs, the run without GF correctly showed intense echo in central Iowa, although the coarseness of the grid prevented realistic bowing structure from being simulated. The 25 km run with GF, however, was not nearly as good, with the echo over Iowa being greatly diminished and the main area of reflectivity being weaker and pushed north into southern Minnesota. For the 13 km runs, differences were much smaller between the runs without GF and with GF. Both runs resembled observations well, showing a bowing echo in Iowa, although the run using GF had more intense echo along the bowing segment. In the 3 km simulations, the differences were enormous. The run not using GF had its most organized convection in eastern IL arcing toward St. Louis, several hundred kilometers in front of where the observed system was. This poor forecast was due to the fact that storms initiated during the evening prior to this day and moved through Iowa during the night and early morning hours (Fig. 12). In the run with GF, intense convection was present in southeastern Iowa, with just a small displacement error to the south. Although a bowing segment is not obvious at this time, it was present in the hours preceding this time. This run was able to correctly depict the most intense storms in Iowa because it did not produce strong storms during the previous night (Fig. 12).

Figure 12 shows the evolution of observed and simulated reflectivity over the derecho event. During the night (0600, 0900, 1200 UTC), the 3 km FV3 run without the GF scheme incorrectly showed extensive convection organizing and moving through Iowa. The 3 km FV3 run with the GF scheme instead had only light areas of reflectivity in Iowa, with most of its stronger convection forming farther west, which is more similar to what was observed. After 1200 UTC, including 1500, 1700 and 2100 UTC, a pronounced bowing echo develops in Iowa and moves east in the 3 km run with GF. Almost no active convection in present in the areas where it was observed from 1700-2100 UTC in the 3km run that did not use GF. Based on conversations with other researchers who have looked at the failure of other models to accurately simulate this event, it appears the incorrect depiction of storms in the previous night is responsible for the poor forecasts (personal communication, P. Skinner, CIMMS, E. Szoke, NOAA/GSL, J. Duda, NOAA/GSL). This is verified by a comparison of the CAPE fields during the morning in Iowa when the derecho was organizing and intensifying (Fig. 13). The 3 km run without GF has almost no CAPE in Iowa (Fig. 13e), whereas the 3 km run with GF shows very high values at 15 UTC (Fig. 13f), exceeding 3,000 J/kg in some areas. Similar results were true for the 13 and 25 km runs, no matter whether they used GF (Fig. 13a-d), and these results match SPC mesonalyses from the morning of the event (Fig. 13g).

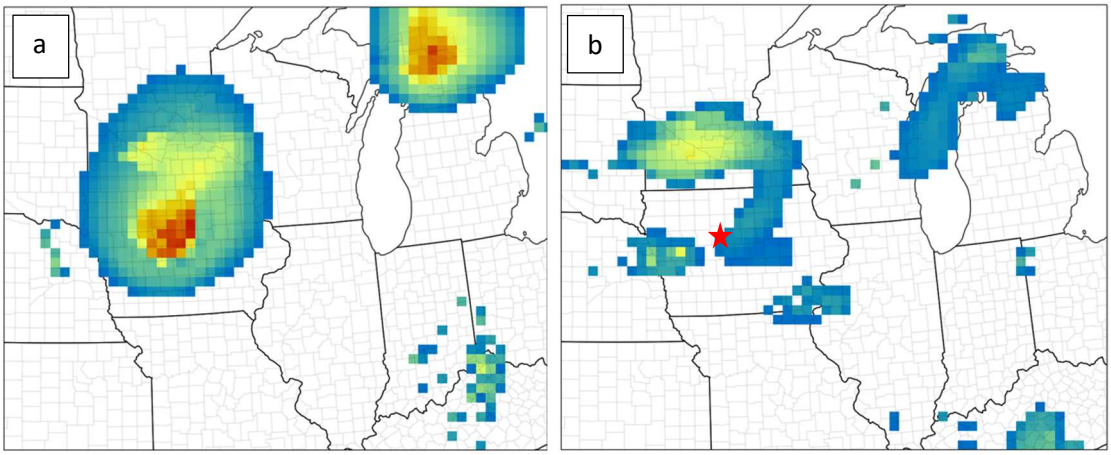

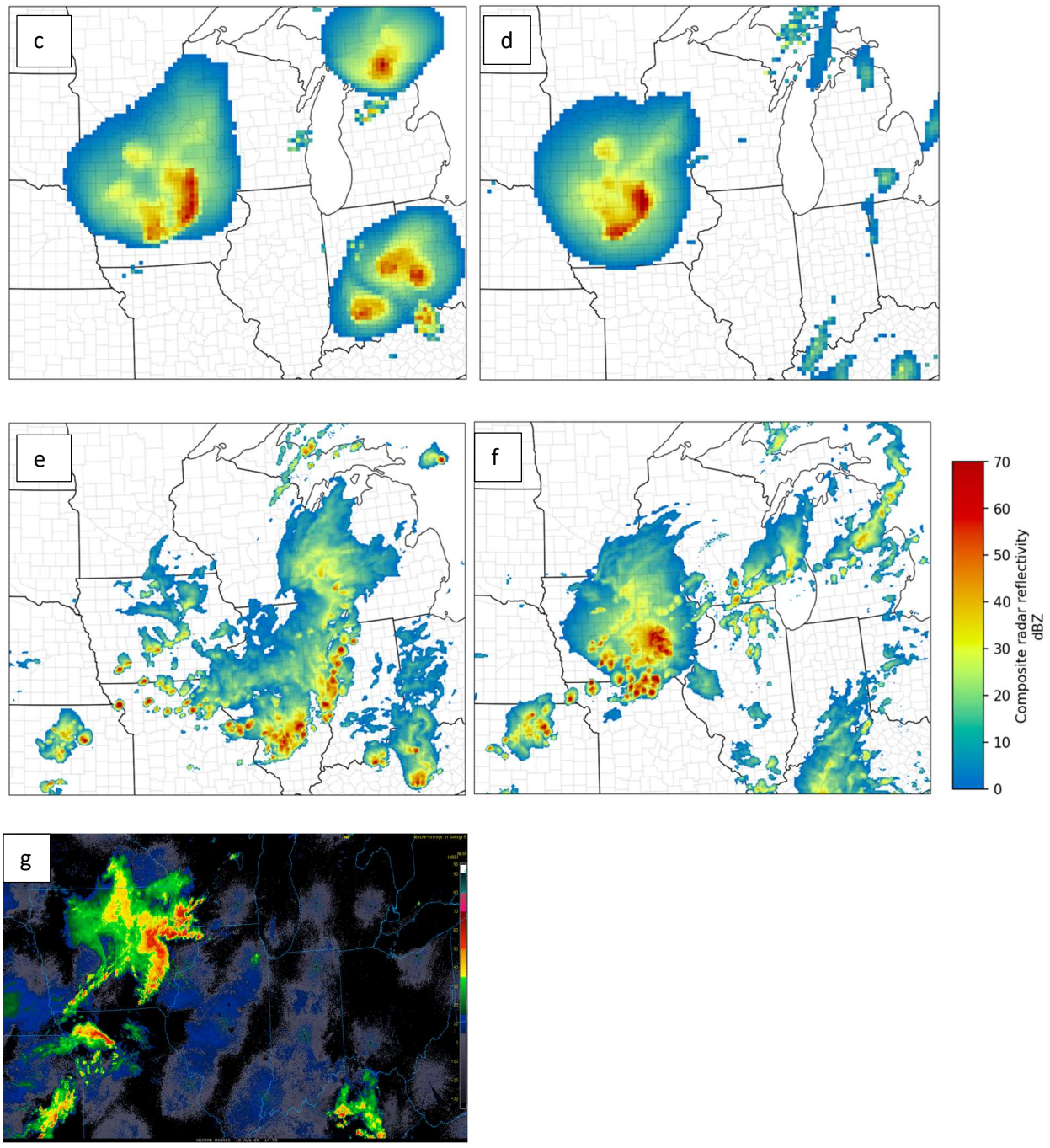

Figure 11: Simulated reflectivity (see color bar at right) at 1800 UTC for the RRFS runs initialized at 0000 UTC 10 August 2020 for a) 25 km without GF, b) 25 km with GF, c) 13 km without GF, d) 13 km with GF, e) 3 km without GF, and f) 3 km with GF. Panel g) shows the observed radar valid at this time.

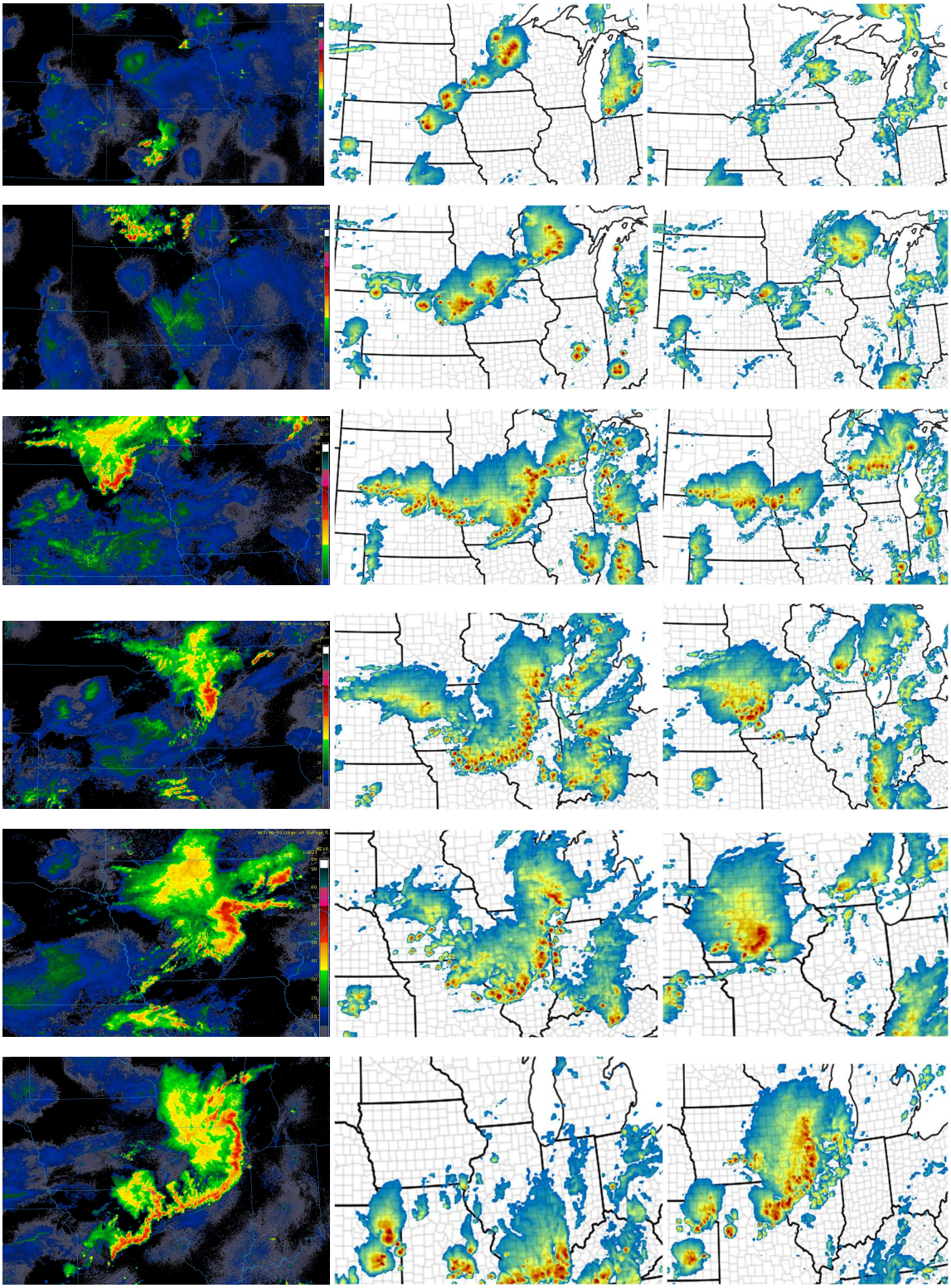

Figure 12: Observed reflectivity (left), and simulated reflectivity from the 3 km RRFS run without the GF scheme (middle column) and the RRFS run with the GF scheme (right column) at 06 UTC (top row), 0900 UTC (second row), 1200 UTC (third row), 1500 UTC (fourth row), 1700 UTC (fifth row), and 2100 UTC (bottom row) 10 August 2020.

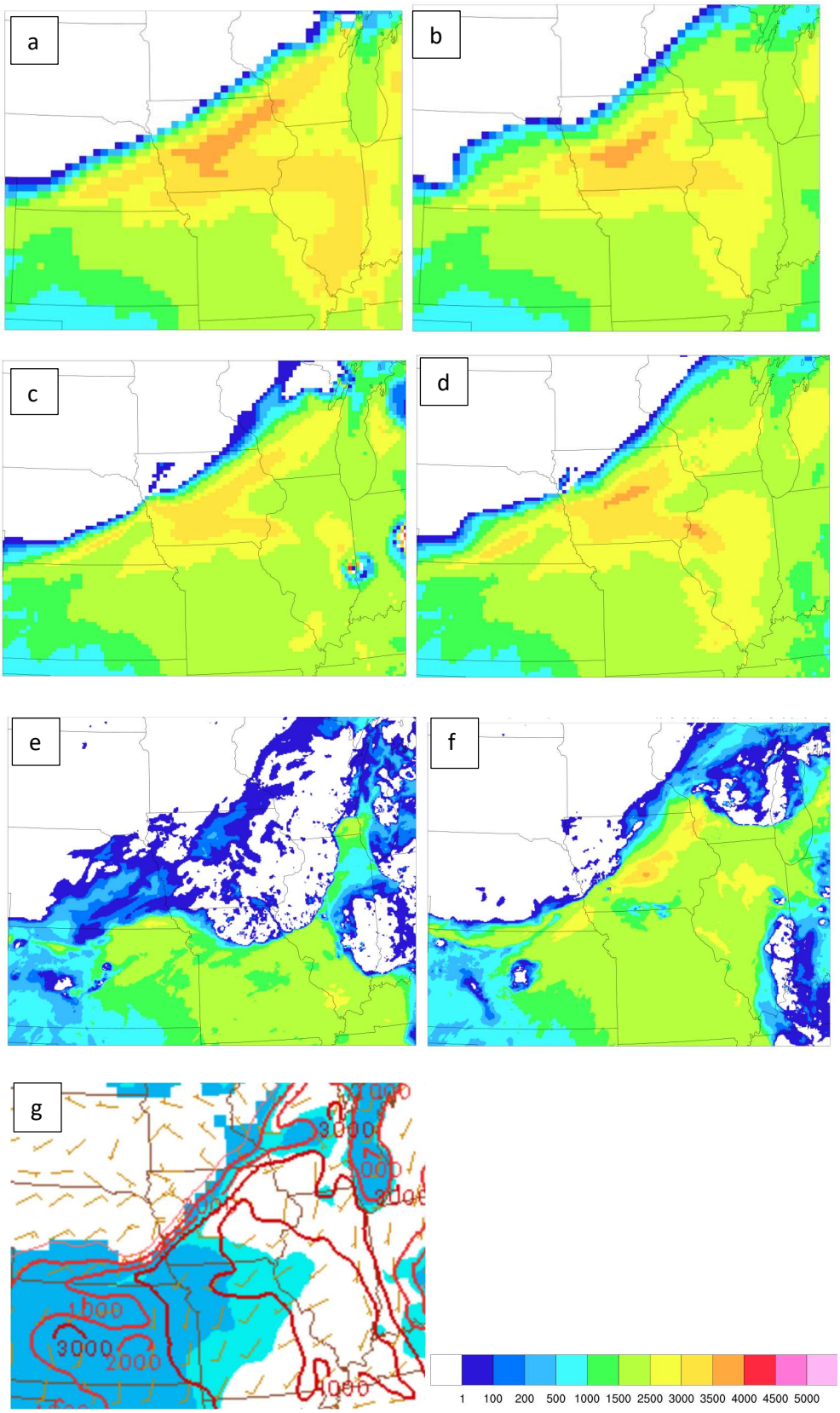
a
b
c
d
e
f
g
3000
2000
1000
1 100 200 500 1000 1500 2500 3000 3500 4000 4500 5000

Figure 13: Simulated CAPE at 1500 UTC for the RRFS runs initialized at 0000 UTC 10 August 2020 for a) 25 km without GF, b) 25 km with GF, c) 13 km without GF, d) 13 km with GF, e) 3 km without GF, and f) 3 km with GF. Values in J kg^{-1} indicated in a-f by color bar in lower right. The observed CAPE valid at this time (from SPC mesoanalysis archive) is shown in panel (g) with red contour intervals of 1000 J kg^{-1} with convective inhibition shaded (light blue 25 J kg^{-1} and darker blue 100 J kg^{-1}), and surface winds overlaid.

These results are unusual in that it is normally believed a convective parameterization is most needed for coarser resolutions and can be neglected for convection-allowing grid spacings. For this case, the coarsest runs (25 km grid spacing) had worse forecasts when the GF scheme was used, while the finest run (3 km grid spacing) benefitted greatly from the use of the GF scheme, albeit not because the scheme was needed to trigger the event of interest, but instead because the GF scheme prevented spurious convection from forming during the prior night, which had resulted in poor depictions of the environment present during the morning when the derecho event formed. The GF scheme only produced very light rainfall amounts during the first few hours of the simulation, typically under 1 mm in most areas (not shown), and these rather broad regions were not supported by observations, but the activation of the scheme led to a much better simulation of the later derecho.

An examination of CAPE and CIN during the hours around when the spurious convection formed showed no noticeable differences between the runs with and without the GF scheme. However, vertical velocities did differ substantially in the region where spurious convection formed, around the time that convection began to trigger (Fig. 14). In the 3 km run without GF, upward motion was much stronger, with values approaching 1 m s^{-1} in some regions where storms would soon initiate. In the run with GF, the values were generally 40 cm s^{-1} or less. The weaker ascent was likely related to the impact the activation of the GF scheme had in a narrow layer around 700 hPa where it caused slight warming and drying (Fig. 15a). Such warming and drying with the GF scheme is due to compensating subsidence, and is often maximized at around 700 hPa (G. Grell, NOAA, 2023, personal communication). Although the impact may seem small at first glance, these changes have a large impact on the amount of lift needed to allow the elevated parcels that were experiencing the least CIN, such as at around 800 hPa, to rise to their level of free convection. The amount of lift needed to reach the level of free convection increased from around 50 hPa in the run that did not use GF to around 110 hPa in the run that did use GF. Of note, the soundings for the region in the 13 and 25 km runs were even more favorable for convective initiation (Fig. 15b), but it likely did not happen because the vertical velocities resolved on these coarser grids are much smaller than in the 3 km runs.

In closing, it should be pointed out how extreme the simulated bow echo became in this 3 km FV3-LAM run that used the GF scheme. At 17 UTC, for instance, 2 m temperatures in the heart of the cold pool fell as low as 11 C, whereas the ambient temperatures ahead of the cold pool were around 28 C, so that a gradient of 17 C existed over a distance of only about 50 km (Fig. 16). Sustained 10 m winds were as high as 70 knots at the time, and the gusts in the model reached 95-100 knots. Winds at 950 and 925 hPa, only about 250-500 m AGL, were as high as 115 knots (Fig. 17). Rainfall of 75-100 mm occurred in a very narrow swath, with much of the rain occurring in only an hour or less. The rainfall amounts were overestimated compared to observations, but sustained winds of over 70 knots were measured in many areas, and peak gusts were measured as high as 109 knots, with estimates based on damage as high as 122 knots. Thus, the values being simulated by the FV3 were in good agreement with what happened in this extreme event.

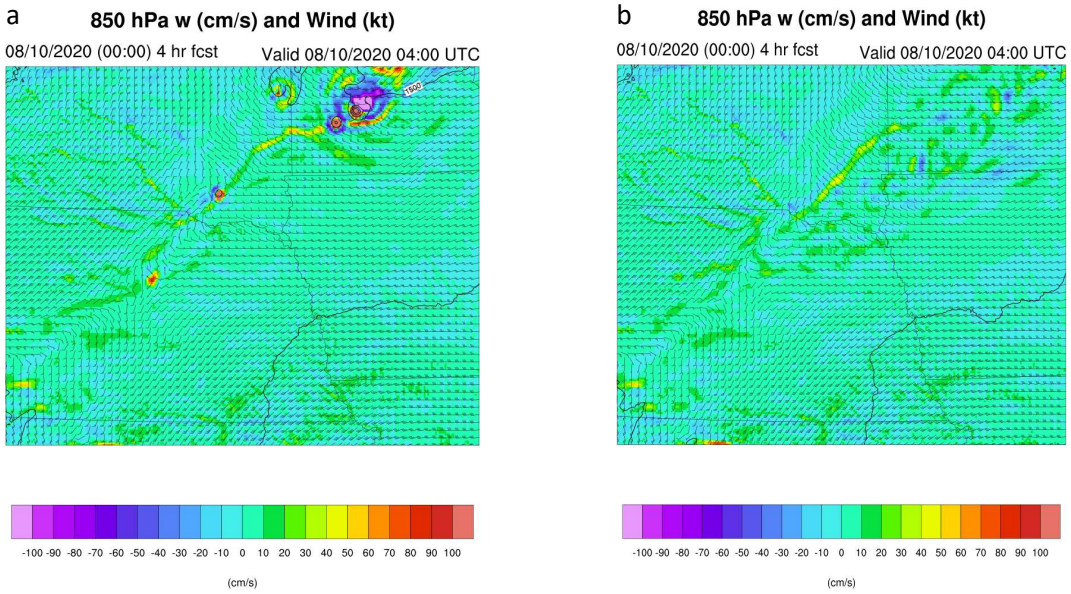

Figure 14: Vertical motion (cm/s, see color scale below figures for magnitudes) at 0400 UTC from the 3 km FV3 run initialized at 0000 UTC 10 August 2020 a) without GF and b) with GF.

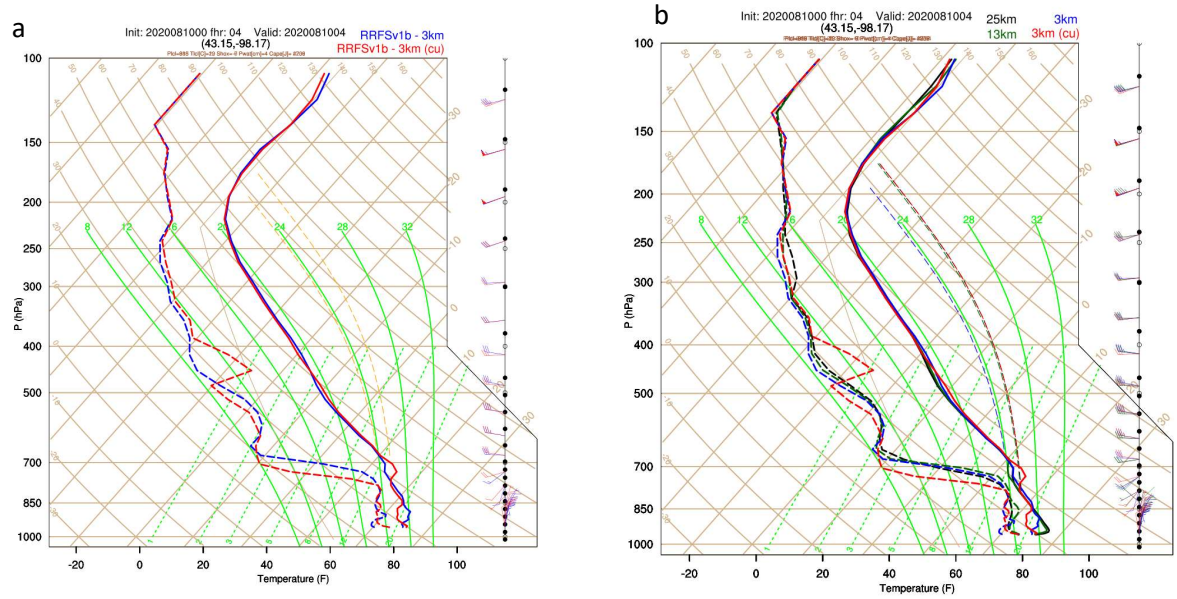

Figure 15: Soundings valid at 0400 UTC from a) the two 3-km runs with blue indicating the run without the GF scheme, and red the run with the GFS scheme, and b) the same but adding the 13 km (dashed black) and 25 km (solid black) results for FV3-LAM initialized at 0000 UTC 10 August 2020.

It is of some interest to compare the peak winds within the simulated strong convective system in Iowa when different horizontal grid spacings are used to understand how sensitive the winds are to changes in resolution, although it is likely operational forecasters would only be examining CAM output for guidance on severe convective hazards. The peak 10-m and 950-hPa winds simulated in the best-performing run using RRFS physics at each of the three

horizontal grid spacings, while the convective system was most intense over Iowa during the period 1700 – 2000 UTC, is shown in Table 1. A pronounced increase in peak winds occurs as the grid spacing is refined, although even with 13 km and 25 km grid spacing, the winds associated with the convective system were strong, with severe intensity at 10 m in the 13 km run, and at 950 hPa in the 25 km run, with 10-m winds just below severe intensity.

Horizontal Grid Spacing (km)	Peak 10-m wind (m s^{-1})	Peak 950-hPa wind (m s^{-1})
25	23.5	29.4
13	31.6	59.7
3	41.8	64.6

Table 1: Peak sustained wind speed (based on instantaneous hourly values) during the period 1700 – 2000 UTC at 10 m and 950 hPa from the best-performing simulations using RRFS physics at 25, 13, and 3-km horizontal grid spacing. For the 25 km run, this was without GF, and for the 13 and 3 km runs, it was with GF.

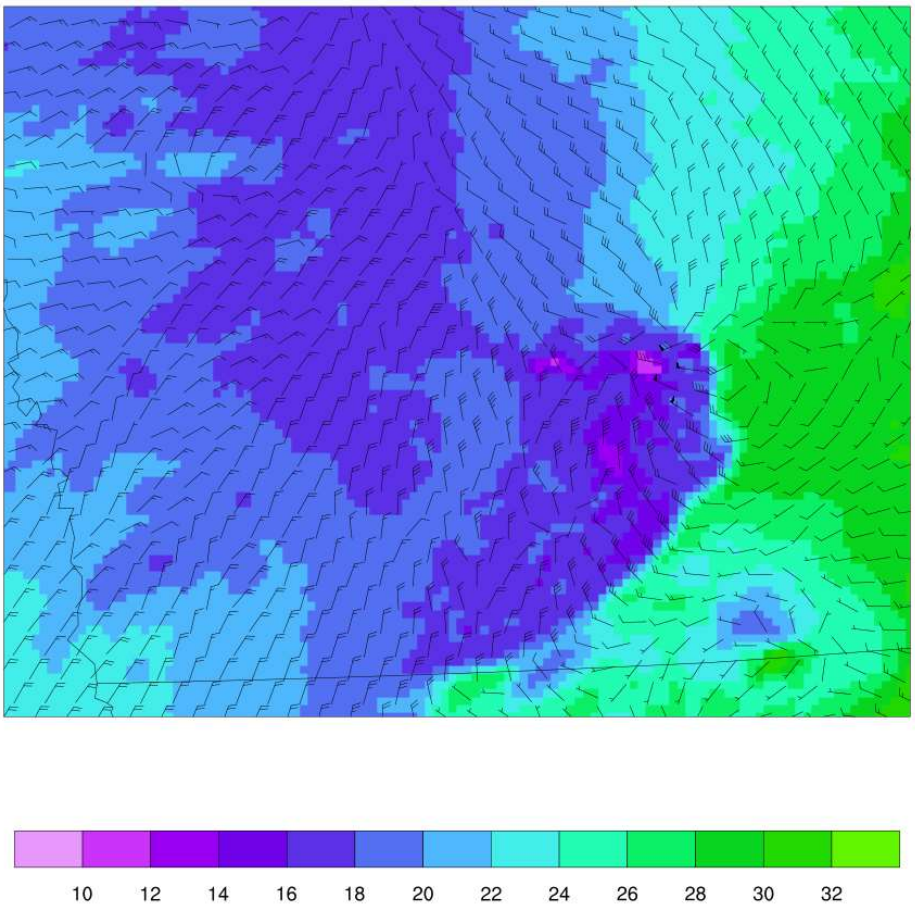

Figure 16: 2m temperatures (°C, see color bar below figure) and 10 m winds (barbs in knots) valid at 1700 UTC in the 3 km RRFS run using the GF scheme.

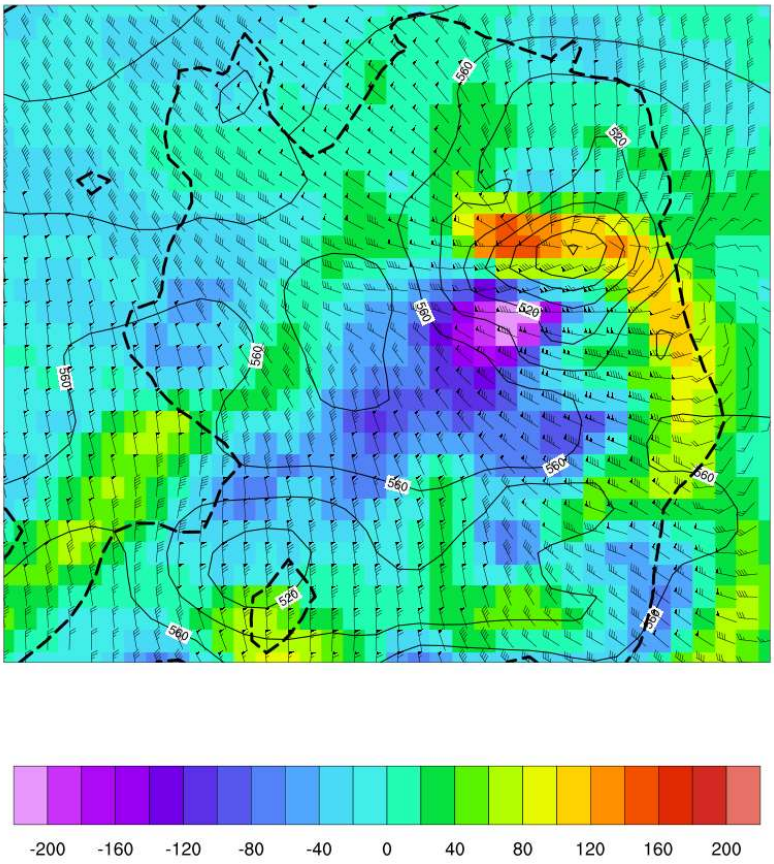

Figure 17: Vertical motion (cm s^{-1}, see color bar below figure), geopotential heights (black contours in m) and winds at 950 hPa (plotted every 3 km) over a portion of central Iowa at 1700 UTC in the 3-km RRFS run using the GF scheme. The 40-dBZ contour of simulated reflectivity is shown with a thick dashed black line.

Summary and Discussion

Three convective cases were simulated using FV3-LAM at three different horizontal grid spacings, 25, 13, and 3 km, and two different physics suites: RRFS, and GFS. The three cases were chosen based on the performance of other models, so that one case had generally been simulated well, one poorly, and for another, performance varied depending on the microphysics scheme used.

Regarding scale awareness of the physics package, rather large differences in the simulations suggests that the physics schemes are not particularly scale-aware. In the 2015 northern Plains bow echo case, a bow echo that propagated south of the Dakotas did not occur until grid spacing was reduced to 3 km in both physics suite runs. In contrast, the 2019 case was better simulated with all model configurations showing convection in roughly the right location, with the biggest differences being in the intensity of the narrow squall line in Texas, which was resolved best at 3 km, as would be expected with a narrow line of storms. In this event, the depiction of the squall line differed more between the two physics suites, with the GFS suite producing a broader, less-defined, squall line. In the derecho 2020 case, extremely large differences were present as the grid spacing changed, but not in the manner usually observed. Because spurious nocturnal convection the night before the derecho impacted simulation of the derecho itself, model performance when the GF cumulus scheme was not used in the RRFS physics suite was better

with the coarser resolutions than the 3 km resolution. When the GF scheme was turned on, the 25 km results were worsened, despite both versions of the model correctly minimizing nocturnal convection prior to the derecho. With 13 km grid spacing, the GF scheme did not change the results substantially, although a slightly better defined bow echo was present in the run using GF. The 3 km run without the GF scheme triggered much spurious convection the night before, so that no derecho was produced, and this simulation was by far the worst of the runs using the RRFS physics suite. However, when GF was turned on in the 3 km run, the best simulation of the derecho of all FV3 runs performed was produced. The GF scheme did produce some spurious precipitation during the night, but it was very light and did not reduce the CAPE over Iowa, so that a very intense bowing line formed the next day, with relatively small timing and location errors. Peak 10 m winds reached 70 knots at two different hours, with gusts to 100 knots. Simulations using the GFS suite did not have a problem at 25 km, and both the 13 and 25 km runs did a reasonable job of showing intense echo over Iowa. As in the 2019 Texas case, the GFS suite produced more of a blob of precipitation with less definition than what happened when the RRFS suite was used at these coarser grid spacings. The 3 km run was even worse than the 3 km RRFS that ran without GF. Spurious convection covered an even greater area the night before the derecho, and the state of Iowa was nearly clear of any echo at the time when the damaging derecho was occurring.

Deliverables

In addition to a seminar given virtually to NCAR during April 2021 and again in December 2021, research results have been presented at the American Meteorological Society's 28th Conf. on Numerical Weather Prediction held virtually in Houston, TX in January 2022, the 25th annual National Weather Association Severe Storms and Doppler Radar Conference held in Des Moines, IA in April 2022, and at the European General Assembly in Vienna, Austria in April 2022. Results were also presented at the 30th Conference on Severe Local Storms held in Santa Fe, NM in October 2022. The PI and Michelle Harrold at DTC have submitted a manuscript on the 2020 derecho simulations to Weather and Forecasting, and it has been conditionally accepted.

References

Chen, C. H., T. Wang, Y. K. Tan, et al., 2009: Research of multi-model short-range ensemble forecasting techniques in forecasting rainy season over Changjiang–Huaihe basin in 2003. *J. Trop. Meteor.*, **25**, 449–457. DOI:10.3969/j.issn.1004-4965.2009.04.010.

Clark, A. J., W. A. Gallus, Jr., M. Xue, and F. Kong, 2010: Growth of spread in convection-allowing and convection-parameterizing Ensembles. Wea. Forecasting, **25**, 594-612.

Davis, C., B. Brown, and R. Bullock, 2006a: Object-based verification of precipitation forecasts. Part I: Methods and application to mesoscale rain areas. Mon. Wea. Rev., **134**, 1772-1784.

Davis, C., B. Brown, and R. Bullock, 2006b: Object-based verification of precipitation forecasts. Part II: Application to convective rain systems. Mon. Wea. Rev., 134, 1785-1795.

Davis, C., B. Brown, R. Bullock, and J. Halley-Gotway, 2009: The Method for Object-based Diagnostic Evaluation (MODE) applied to numerical forecasts from the 2005 NSSL/SPC Spring Program. Wea. Forecasting, **24**, 1252-1267.

Gallus, W. A., Jr., 2010: Application of object-oriented verification techniques to ensemble precipitation forecasts. Wea. Forecasting. **25**, 144-158.

Gallus, W. A., Jr. and M. Harrold, 2023: Challenges in Numerical Weather Prediction of the 10 August 2020 Midwestern Derecho: Examples from the FV3-LAM. Wea. Forecasting. (conditionally accepted).

Johnson, A., X. Wang, M. Xue, and F. Kong, 2011: Hierarchical cluster analysis of a convection-allowing ensemble during the Hazardous Weather Testbed 2009 Spring Experiment. Part II: Ensemble clustering over the whole experiment period. Mon. Wea. Rev., 139, 3694-3710.

Li, X., H. R. He, C. H. Chen, 2017: A convection-allowing ensemble forecast based on the breeding growth mode and associated optimization of precipitation forecast. J. Meteor. Res., 31 (5), 955-964. Doi: 10.1007/s13351-017-6695-0.

Stensrud, D. J., J. Bao, and T. T. Warner, 2000: Using initial conditions and model physics perturbations in short-range ensemble simulations of mesoscale convective systems. Mon. Wea. Rev., 128, 2077–2107.